

Control Policies for Operational Coordination of Electric Power and Natural Gas Transmission Systems

Anatoly Zlotnik, Line Roald, Scott Backhaus, Michael Chertkov, and Göran Andersson

Abstract—The abundance of natural gas in the United States and the need for cleaner electric power have prompted widespread installation of gas-fired power plants and caused electric power systems to depend heavily on reliable gas supplies. The use of gas generators for peak load and reserve generation causes high intra-day variability in withdrawals from high pressure gas transmission systems, which leads to gas price fluctuations and supply disruptions that affect electric generator dispatch and threaten the security of both power and gas systems. In this manuscript, we investigate different gas compressor operation policies and their influence on the affected power system. Specifically, we consider constant pressure boost ratios and dynamic adjustment of these ratios to track pressure set-points. We also implement a joint optimization of generator dispatch schedules and gas compressor protocols using a dynamic gas flow model. We develop tractable, physically accurate implementations that are compared using an integrated model of test networks for power and gas systems with 24 and 25 nodes, which are coupled through gas-fired generators. This demonstrates the benefits that can be achieved with globally optimized gas system operations and increased gas-electric coordination.

I. INTRODUCTION

Natural gas is increasingly used for electricity generation, which has facilitated the retirement of older coal and nuclear power plants and integration of renewable resources [1]. The expansion in gas-fired generators (GFGs) to over 40% of total capacity in North America has brought environmental and efficiency benefits, but also created a dependence on gas simultaneously with vulnerabilities in the natural gas supply chain [2]. Fuel usage of GFGs is determined by generation schedules in the day-ahead electricity market, which is cleared by an independent (electric) system operator (ISO) by solving the optimal power flow (OPF) problem [3], [4]. Single cycle GFGs can quickly go online and modulate output, and are used as marginal resources that start and shut down multiple times a day. This creates highly variable withdrawals from gas pipeline networks (GPNs).

Natural gas was historically withdrawn from transmission systems with little intra-day variation by local distribution companies (LDCs) that purchase firm delivery contracts [5]. In contrast, GFGs usually purchase short-term gas contracts that may be subjected to scheduling restrictions or interrupted. When this happens, ISOs must change their planned intra-day operations, which can impact system security or

increase costs. ISOs are therefore challenged to meet demand, maintain operating reserves, and ensure power system reliability. Conversely, GFGs play a complex role in natural gas markets because their demand is price sensitive.

Despite growing concerns about the lack of gas and power system coordination [6], adapting market timing, regulation, and physical operations remains problematic [7]. Infrastructure expansion and market synchronization do not advance current practices for physical GPN operations to react to generator requirements or improve coordination across systems and regions [8]. The main control variables available to gas pipeline operators (GPOs) are protocols for gas compressor stations (GCSs), which boost flow to compensate for dissipative friction effects in pipelines. Policies are regionally fragmented and usually ad-hoc reactions to local conditions [8]. Optimization of steady-state compression protocols has been formalized in optimal gas flow (OGF) problems [9], [10], which determine optimal constant GCS set-points for balanced injections and withdrawals over a network while satisfying system pressure constraints.

Because of increasing GFG construction, the steady-state assumption no longer realistically represents short-term operating conditions. Extending the OGF to variable and unpredictable gas withdrawals requires dynamic modeling and optimal control strategies. However, GPN dynamics are notoriously difficult to simulate and optimize in an efficient way [11], [12]. In related optimization problems, the partial differential equations (PDEs) for gas flows comprise constraints that must be satisfied over widely distributed space and time domains, and their nonlinearity makes computational tractability a hurdle. New models that incorporate the physics of gas pipelines [13] and networks [14] were recently developed and validated by comparison with traditional numerical PDE methods. They were used to extend the OGF to dynamic flows involving time-varying gas withdrawals by representing the PDE constraints in the resulting optimal control problems (OCP), which was solved numerically after discretization to a nonlinear program (NLP) using pseudospectral (PS) approximation.

Joint optimization for operational planning for power and gas infrastructures was previously studied, including joint gas-electric OPF [15], [16], unit commitment with gas security constraints [17], [18], and multi time-period scheduling [19], [20]. Those studies rely on the steady-state Weymouth equations, which do not capture the dynamic fluctuations that lead to intra-day gas supply issues, or use simple finite-difference approximations that may create scaling issues. To enable coordination, optimization and control techniques

A. Zlotnik, M. Chertkov and S. Backhaus are with Los Alamos National Laboratory, Los Alamos, NM 87544. Email: {zlotnik | chertkov | backhaus}@lanl.gov. L. Roald and G. Andersson are with the Power Systems Laboratory at the Department of Electrical Engineering, ETH Zurich, Switzerland. Email: {roald | andersson}@eeh.ee.ethz.ch.

must use dynamic GPN models that are physically realistic on the time-scale of ISO operations.

In this study, we demonstrate the feasibility of rapidly optimizing power and gas flows in integrated systems with GFGs that cause rapidly varying, high volume gas flow transients. Moreover, in addition to formulating separate and combined optimization problems based on static and dynamic gas system models, respectively, we contrast the two distinct modes of GCS operation. Specifically, while both modes use globally optimized constant boost ratios, one applies the ratio and another adjusts the boost to track the nominal compressor outlet pressure. We propose a computational methodology to solve each scenario, and compare them by quantifying operational cost and feasibility using a case study of interacting gas and electricity test models.

The manuscript is organized as follows. In Section II, we summarize the co-optimization and compressor operation cases to be examined and describe the test systems. In Section III, we describe how generator dispatch is obtained based on an OPF. Section IV reviews a recent method to model a GPN with gas compressors as a reduced control system model. In Section V, we describe schemes for separate and combined day-ahead optimization of generator dispatch and gas pipeline operations. In Section VI we compare the scenarios under different compressor operation protocols and stress levels, and Section VII concludes the study.

II. COORDINATION SCENARIOS AND TEST SYSTEM

We consider three paradigms for operational planning for integrated electric power and natural gas systems.

Scenario A: Approximates current practice. Power system operation ignores gas system impacts. Given generator dispatch schedules, GFGs calculate average gas usage and contract constant-rate delivery from the GPN. The GPO calculates constant compression ratio set-points using a steady-state model, and checks system feasibility by simulation.

Scenario B: Distributed control of compressors. As in Scenario A, GFGs contract gas required for their generation schedule from the GPN. The GPO calculates constant set-points for compressor outlet pressure assuming a steady-state model, and checks system feasibility by simulation where compressors adjust ratios dynamically to track the set-points.

Scenario C: Gas-aware power system operation. The ISO mitigates congestion in the gas system by adjusting GFG fuel usage to conform with gas system limitations. This allows the GPO to operate compressors at constant boost ratios as in current practice, but the ISO would need gas system models and data, which requires regulatory and market changes.

The case studies use the 24-node IEEE One Area RTS-96 test network [22] coupled with a 24-pipe LANL benchmark gas system test network, which was used in a gas network control study [14], as illustrated in Figure 1. The production limits of generators in the power system network are scaled so that total generation capacity is 2724 MW. Line capacities are reduced to 50%, system loads are scaled to 80% of nominal values, and some loads are scaled with one of two time-varying curves (A or B) inset at top left in Figure 1.

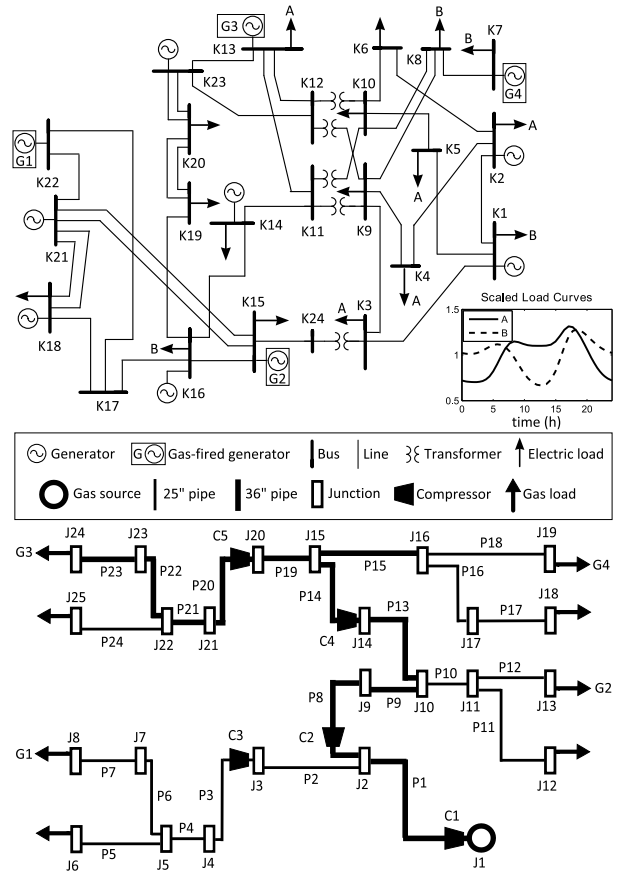


Fig. 1. Schematic of integrated electric and gas test networks. IEEE RTS96 One Area 24 node power system test network (top) coupled with the LANL benchmark 25 node gas system test network (bottom) through GFGs (G1 to G4). Electric loads marked with A or B are scaled by the time-varying load curves in the inset plot at right. Electric buses (K1 to K24), gas pipes (P1 to P24), pipe junctions (J1 to J25), and gas compressors (C1 to C5) are indicated. Data available online [21].

For the baseline case, remaining constant electric loads are scaled to 50% of nominal values. We place gas-fired shoulder plants at buses 7 and 13, and peak power plants at 15 and 22, for which costs $c(p_i) = c_g q(p_i)$ of generations p_i are based on gas usage according to a heat rate curve

$$q(p_i) = q_0 + q_1 p_i + q_2 p_i^2. \quad (1)$$

The quadratic coefficients (q_0, q_1, q_2) are (3.08, 0.48, 0.001) and (7.83, 0.26, 0.0015) for peaking and shoulder plants, respectively [23], and a gas price of $c_g = 6$ \$/mmBTU is used. Cost coefficients for other generators are obtained from MatPower [24]. GFGs at power system nodes 22, 15, 13, and 7 draw fuel from gas system junctions 8, 13, 24, and 19, respectively. The friction factor and sound speed parameters used for the gas pipelines are $\lambda = 0.01$ and $a = 377.968$ m/s. The integrated model is scaled so that 40% of generating capacity is gas-fired, and approximately 50% of gas is used for power in the baseline case. LDCs at gas system junctions 6, 12, 18, and 25 each use the remaining gas at a mean rate of 40 kg/s, weighted by the A profile in the inset plot in Figure 1. Gas is available at junction J1 at 500 psi, and boosted into the system by compressor C1, with total daily throughput of $\approx 500,000$ mmBTU. Pressure and compression

ratios are bounded in [500, 800] psi and [1, 2], respectively.

III. ELECTRIC POWER SYSTEM OPERATION

ISOs such as PJM [4] clear the market by solving optimal power flow (OPF) and unit commitment problems [3] to obtain hourly generation schedules for the following day. We estimate this mechanism by solving an OPF where demand and production are continuous functions of time in order to model generator dispatch response to intra-day load variation. The result is used to approximate GFG fuel consumption, and enables mathematical integration with the smooth dynamic gas flow model in Section V.

Because gas withdrawals are determined by the active power generation, we model power system flows using the DC approximation, which agrees with previous integration studies [15], [17]. For simplicity, we disregard line outage, ramping, and unit commitment constraints, but note that they (and the AC power flow equations) can be incorporated.

We formulate the continuous-time DC OPF as an extension to the standard single time-step formulation [25]. Let $\mathbb{G}_P = (\mathcal{V}_P, \mathcal{E}_P)$ represent the graph of the power network, where \mathcal{V}_P is the set of nodes with $|\mathcal{V}_P| = m$ and \mathcal{E}_P is the set of edges/lines of the system with $|\mathcal{E}_P| = n$. The set of generators is denoted by \mathcal{G} . To simplify notation, we assume that there is one generator with production $p_i(t)$ and one demand with consumption $h_i(t)$ per node, such that $|\mathcal{G}| = |\mathcal{V}_P| = m$. The demands $h_i(t)$ are given as continuous demand functions defined for $0 \leq t \leq T$ where $T = 24$ hours. The power flows from bus i to bus j are denoted by f_{ij} , with maximum values of \bar{f}_{ij} . The objective is to minimize the total cost of generation over the time horizon $[0, T]$ where $c_i(p_i(t))$ are cost functions for production, i.e.,

$$J_P \triangleq \sum_{i \in \mathcal{G}} \int_0^T c_i(p_i(t)) dt. \quad (2)$$

The constraints $\forall t \in [0, T]$ for total system power balance, generator production limits, and power flow limits are

$$\sum_{i \in \mathcal{V}} (p_i(t) - h_i(t)) = 0, \quad (3)$$

$$0 \leq p_i(t) \leq p_i^{max}, \quad \forall i \in \mathcal{G}, \quad (4)$$

$$-\bar{f}_{ij} \leq \mathbf{M}_{(ij, \cdot)}(p(t) - h(t)) \leq \bar{f}_{ij}, \quad \forall \{ij\} \in \mathcal{E}_P, \quad (5)$$

where $p(t)$ and $h(t)$ are vector functions containing $p_i(t)$ and $h_i(t)$, respectively. The matrix $\mathbf{M} \in \mathbb{R}^{n \times m}$ relates the line flows to the nodal power injections, and is defined as

$$\mathbf{M} = B_f \begin{bmatrix} (\tilde{B}_{bus})^{-1} & \mathbf{0} \\ \mathbf{0} & \mathbf{0} \end{bmatrix} \quad (6)$$

where B_f and \tilde{B}_{bus} are line and bus susceptance matrices, where \tilde{B}_{bus} lacks the column and row corresponding to the slack bus [26]. $\mathbf{M}_{(ij, \cdot)}$ is the row of \mathbf{M} related to line $(ij) \in \mathcal{E}_P$. The continuous-time DC OPF is then given by

$$\begin{aligned} \min_{p(t)} \quad & J_P \text{ in (2)} \\ \text{s.t.} \quad & \text{power system constraints: (3) - (5)} \end{aligned} \quad (7)$$

The dispatch solutions $p_i(t)$ are translated into GFG gas usage curves $d_i(t) = q(p_i(t))$ using (1). Next, we describe how the effects of gas withdrawals on the GPN are modeled.

IV. MODELING OF GAS NETWORK DYNAMICS

We use a reduced model for the dynamics of a GPN actuated by nodal compressor stations [14]. The GPN is represented as a directed graph $\mathbb{G} = (\mathcal{V}, \mathcal{E})$, where edges (pipes) $\{i, j\} \in \mathcal{E}$ connect nodes (junctions) $i, j \in \mathcal{V}$. The state on the edge $\{i, j\}$ is given by the density ρ_{ij} and flux φ_{ij} defined on a time interval $[0, T]$ and the distance variable $x_{ij} \in [0, L_{ij}]$, where L_{ij} is the length of edge $\{i, j\}$.

Assuming slow transients that do not excite shocks or waves, the flow of gas on the edges is described by a simplification of the Euler equations in one dimension [27], given after nondimensionalization [14] by

$$\partial_t \rho_{ij} + \partial_x \varphi_{ij} = 0, \quad \forall \{i, j\} \in \mathcal{E} \quad (8)$$

$$\partial_t \varphi_{ij} + \partial_x \rho_{ij} = -\frac{\lambda_{ij} \ell}{2D_{ij}} \frac{\varphi_{ij} |\varphi_{ij}|}{\rho_{ij}}, \quad \forall \{i, j\} \in \mathcal{E} \quad (9)$$

The parameters are the friction factor λ , pipe diameter D , speed of sound a , and nondimensionalization scaling ℓ . The term on the right hand side of (9) aggregates friction effects. We assume isothermal flow in which gas pressure p and density ρ are related by $p = a^2 \rho$.

Gas compression is modeled as conservation of flow and multiplicative change in density at a point $x = c$, i.e., $\rho(t, c^+) = \alpha(t) \rho(t, c^-)$ and $\varphi(t, c^+) = \varphi(t, c^-)$, where $\alpha(t)$ is a compression ratio. We denote $h(c^-) = \lim_{x \nearrow c} h(x)$ and $h(c^+) = \lim_{x \searrow c} h(x)$. The required power is proportional to

$$C \propto \eta^{-1} |\varphi(t, c)| (\max\{\alpha(t), 1\}^{2m} - 1) \quad (10)$$

with $0 < m < (\gamma - 1)/\gamma < 1$ where γ is the heat capacity ratio and η is the compressor efficiency [9]. We define the controller set $\mathcal{C} \subset \mathcal{E} \times \{+, -\}$, where $\{i, j\} \equiv \{i, j, +\} \in \mathcal{C}$ (resp. $\{j, i\} \equiv \{i, j, -\}$) denotes a controller at node $i \in \mathcal{V}$ (resp. $j \in \mathcal{V}$) that augments the density of gas flowing into edge $\{i, j\} \in \mathcal{E}$ in the + (resp. -) direction. Compression is expressed as a ratio $\alpha_{ij} : [0, T] \rightarrow \mathbb{R}_+$ for $\{i, j\} \in \mathcal{C}$.

We denote by $s_j : [0, T] \rightarrow \mathbb{R}$ the density of gas entering the GPN from a node $j \in \mathcal{V}_S$ in the set of supply terminals called ‘‘slack’’ junctions, able to supply any mass flux at the given density. A mass flux withdrawal (or injection, if negative) at a junction $j \in \mathcal{V}_D = \mathcal{V} \setminus \mathcal{V}_S$ is denoted by $d_j : [0, T] \rightarrow \mathbb{R}$, where \mathcal{V}_D is the set of demand (non-‘‘slack’’) nodes. The functions $\{\alpha_{ij}\}_{\{i,j\} \in \mathcal{C}}$, $\{d_j\}_{j \in \mathcal{V}_D}$, and $\{s_j\}_{j \in \mathcal{V}_S}$ create nodal balance conditions of the form

$$\alpha_{ji}(t) \rho_{jk}(t, 0) = \alpha_{jk}(t) \rho_{ij}(t, L_j), \quad \forall j \in \mathcal{V}_D \text{ and } \{i, j\}, \{j, k\} \in \mathcal{E}, \quad (11)$$

$$d_j(t) = \sum_{i \in \mathcal{V}_D} \varphi_{ij}(t, L_{ij}) - \sum_{k \in \mathcal{V}_D} \varphi_{jk}(t, 0), \quad \forall j \in \mathcal{V}_D, \quad (12)$$

$$\rho_{ij}(t, 0) = s_i(t), \quad \forall i \in \mathcal{V}_S. \quad (13)$$

The reduced model for the network flow dynamics (8)-(9) with nodal conditions (11)-(13) has been formulated by integrating pipe segments as lumped elements [14]. In the

result, let $V = |\mathcal{V}_D|$ and $E = |\mathcal{E}|$ and assign to each edge an index in $[E]$, where $[N] = \{1, \dots, N\}$ for a positive integer $N \in \mathbb{N}$, using the mapping $\pi_e : \mathcal{E} \rightarrow [E]$. Each node in \mathcal{V}_D is assigned an internal density and each edge in \mathcal{E} is assigned a flow, yielding the nodal density and edge flow state vectors $\rho = (\rho_1, \dots, \rho_V)^T$ and $\varphi = (\varphi_1, \dots, \varphi_E)^T$. Here nodal ρ_i and ρ_j are related to $\rho_{ij}(t, 0)$ and $\rho_{ij}(t, L)$ at edge boundaries with nodal compression variables α_{ij} by

$$\rho_{ij}(t, 0) = \alpha_{ij}\rho_i(t) \text{ and } \rho_{ij}(t, L) = \alpha_{ji}\rho_j(t). \quad (14)$$

Each node $j \in \mathcal{V}_D$ is subject to withdrawal flux d_j (that is negative if an injection), forming the vector $d = (d_1, \dots, d_V)^T$. Slack node densities are $s = (s_1, \dots, s_b)^T$, where $b = |\mathcal{V}_S|$. Parameters are contained in the diagonal matrices $\Lambda, K \in \mathbb{R}^{E \times E}$ defined by $\Lambda_{kk} = L_k$ and $K_{kk} = \ell\lambda_k/D_k$, where L_k , λ_k , and D_k are the nondimensional length, friction coefficient, and diameter of edge $k = \pi_e(ij)$.

Define the weighted incidence matrix $B : \mathbb{R}^E \rightarrow \mathbb{R}^V$ by

$$B_{ik} = \begin{cases} \alpha_{ij} & \text{edge } k = \pi_e(ij) \text{ enters node } i, \\ -\alpha_{ij} & \text{edge } k = \pi_e(ij) \text{ leaves node } i, \\ 0 & \text{else} \end{cases} \quad (15)$$

as well as the incidence matrix $A = \text{sign}(B)$. Let $A_s, B_s \in \mathbb{R}^{b \times E}$ denote submatrices of rows of A and B that correspond to \mathcal{V}_S , and let $A_d, B_d \in \mathbb{R}^{V \times E}$ relate similarly to \mathcal{V}_D . Define a function $g : \mathbb{R}^E \times \mathbb{R}_+^E \rightarrow \mathbb{R}^E$ by $g_j(x, y) = x_j|x_j|/y_j$. The reduced network flow (RNF) ODE model is

$$\dot{\rho} = (|A_d|\Lambda|B_d^T|)^{-1}[4(A_d\varphi - d) - |A_d|\Lambda|B_s^T|\dot{s}], \quad (16)$$

$$\dot{\varphi} = -\Lambda^{-1}(B_s^T\dot{s} + B_d^T\dot{\rho}) - Kg(\varphi, |B_s^T|\dot{s} + |B_d^T|\dot{\rho}). \quad (17)$$

For a connected graph, $A_d \in \mathbb{R}^{V \times E}$ and $B_d \in \mathbb{R}^{V \times E}$ are full rank, and therefore $|A_d|\Lambda|B_d^T|$ is invertible. Time-varying parameters are gas withdrawals $d \in \mathbb{R}^V$, input densities $s \in \mathbb{R}_+^b$, and compressions $\alpha_{ij} \in \mathcal{C}$. The RNF (16)-(17) is a consistent spatial discretization of the PDE (8)-(9) [13].

When $\dot{\rho} = 0$, $\dot{\varphi} = 0$, $\dot{s} = 0$, $\dot{d} = 0$, and $\dot{\alpha}_{ij} = 0$ for all $\{i, j\} \in \mathcal{C}$, equations (16)-(17) reduce to

$$A_d\varphi = d, \quad (18)$$

$$\Lambda K(\varphi \odot |\varphi|) = (B_s^T\dot{s} + B_d^T\dot{\rho}) \odot (|B_s^T|\dot{s} + |B_d^T|\dot{\rho}), \quad (19)$$

where \odot denotes the point-wise vector product. This corresponds to steady-state GPN balance laws [9], [14].

V. OPTIMIZATION AND CONTROL SCHEMES

We now describe optimization schemes and control protocols that are implemented for the three considered scenarios.

Scenario A: The ISO solves the OPF (7), and each GFG applies (1) to compute its gas usage schedule. This is averaged and given to the GPO, who computes constant gas compressor set-points by solving the steady-state OGF [9]. For that problem, the optimization objective is to minimize compression costs of the form (10), i.e.,

$$J_G \triangleq \sum_{\{i,j\} \in \mathcal{C}} \frac{|\varphi_{\pi_e(ij)}|}{\eta_{ij}} ((\max\{\alpha_{ij}, 1\})^{2m} - 1). \quad (20)$$

Nodes are subject to steady withdrawals d_j for $j \in \mathcal{V}_D$, available supply densities s_j for $j \in \mathcal{V}_S$, and box constraints

$$\rho_i^{\min} \leq \alpha_{ij}\rho_i \leq \rho_i^{\max}, \quad \forall i \in \mathcal{V}_D \quad (21)$$

$$1 \leq \alpha_{ij} \leq \alpha_{ij}^{\max}, \quad \forall \{i, j\} \in \mathcal{C}, \quad (22)$$

on the density and compression. Steady-state flow balance laws are enforced using (18)-(19), where decision variables α_{ij} for $\{i, j\} \in \mathcal{C}$ are embedded in the weighted incidence matrices B_s and B_d . The static OGF is given by

$$\begin{aligned} \min_{\alpha_{ij}} \quad & J_G \text{ in (20)} \\ \text{s.t.} \quad & \text{flow balance constraints: (18) - (19)} \\ & \text{density \& control constraints: (21), (22)} \end{aligned} \quad (23)$$

To compensate for errors related to steady-state modeling, conservative compression ratios are required to maintain balanced gas flows under actual transient conditions. We multiply the averaged withdrawals by an engineering factor of 1.25 when computing the OGF. The resulting ratios α_{ij} are embedded within the weighted incidence matrices B_s and B_d in (16)-(17) to simulate the gas flows that result when the actual time-varying gas usage is in effect.

Scenario B: The OPF and OGF are computed as in Scenario A. In addition to compression ratios, the steady-state OGF solution yields values of the pressure at compressor outlets, which are used as set-points ρ_{out}^* for dynamic compressor operation. The boost ratios are adjusted to track these set-points according to

$$\alpha(t) = \begin{cases} \alpha_{\min} & \rho_{\text{out}}^*/\rho_{\text{in}} < \alpha_{\min} \\ \rho_{\text{out}}^*/\rho_{\text{in}} & \alpha_{\min} \leq \rho_{\text{out}}^*/\rho_{\text{in}} \leq \alpha_{\max} \\ \alpha_{\max} & \rho_{\text{out}}^*/\rho_{\text{in}} > \alpha_{\max} \end{cases} \quad (24)$$

while remaining within the box constraint $\alpha(t) \in [\alpha_{\min}, \alpha_{\max}] = [1, 2]$. This model of distributed local control illustrates the result of policies that do not anticipate the effect of changes to gas flows elsewhere in the system.

Scenario C: A combined optimization scheme is implemented to represent gas-aware power system operation, where the OPF is optimized together with constant compression ratios for the GPN subject to gas dynamics and density constraints. The latter are now time-dependent, and we use periodic terminal conditions on the state of the gas network (for simplicity), resulting in

$$\rho_i^{\min} \leq \alpha_{ij}\rho_i(t) \leq \rho_i^{\max}, \quad \forall i \in \mathcal{V}_D \quad (25)$$

$$\rho(0) = \rho(T), \quad \varphi(0) = \varphi(T), \quad (26)$$

over the same 24-hour period $[0, T]$ as used in the OPF problem (7). The combined gas-electric OCP is then

$$\begin{aligned} \min_{p(t), \alpha_{ij}} \quad & \beta_P J_P + \beta_G J_G \text{ using (2) and (20)} \\ \text{s.t.} \quad & \text{power system constraints: (3) - (5)} \\ & \text{generator heat-rate coupling equation: (1)} \\ & \text{RNF gas dynamics constraints: (16) - (17)} \\ & \text{gas density \& terminal constraints: (25), (26)} \\ & \text{compression ratio constraints: (22).} \end{aligned} \quad (27)$$

The DC OPF (7) and OGF (now subject to dynamic constraints) are coupled in (27) through the heat rate curve (1),

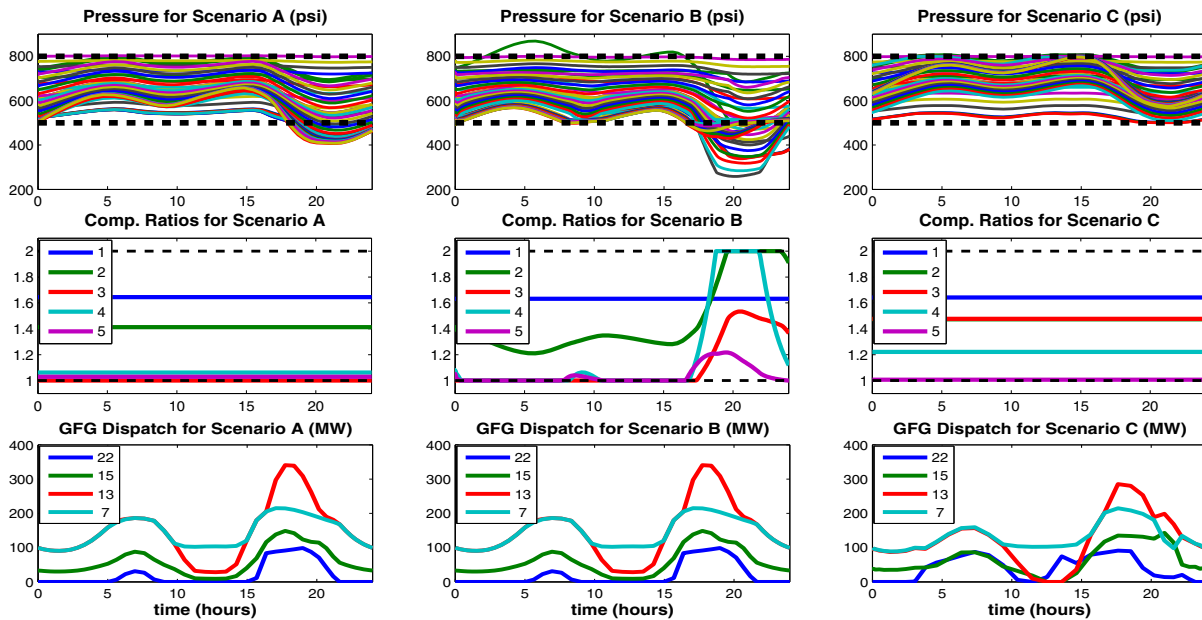


Fig. 2. Comparison of Scenarios A, B, and C (left to right) for the baseline case. From top to bottom: Simulated nodal gas pressures (color) and bounds (dashed); Compression ratios; Gas-fired generator dispatch solutions.

which relates the GFG fuel usage to power output. The scaling coefficients β_P and β_G are used to appropriately weight the power and gas system objectives, respectively. Because we aim to optimize costs for the ISO while maintaining pressure constraint feasibility for the GTS, compression cost is kept a minimal part of the objective (to guarantee a unique solution), choosing β_P and β_G to get $\beta_P J_P \approx 10^2 \beta_G J_G$.

VI. IMPLEMENTATION AND CASE STUDIES

We solve the OPF (7) using a polynomial approximation scheme that will be required to resolve time-dependent GPN dynamics [14], which enables solution of the combined optimization problem (27). The OGF problem (23) is a nonlinear program without time-dependence, where the constraints are algebraic relations. The joint optimization problem (27) is a constrained OCP on a continuous function space with dynamic constraints, which we approximate with a nonlinear program (NLP) obtained using PS discretization [28] on 35 collocation points in time. The decision variables are constant compressor ratios α_{ij} , as well as coefficients of polynomial expansions that approximate the time-varying gas generator dispatch $p(t)$ and gas dynamics solutions $\rho(t)$ and $\varphi(t)$. Transcription from the OCP to the NLP is described in the context of gas networks in previous work [14]. Solutions for problems (7), (23), and (27) are implemented using the interior-point solver IPOPT version 3.11.8 running with the linear solver ma57 [29] by providing functions for the objective, constraints, and their gradients with respect to the decision variables and initializing at feasible random initial conditions. With compression ratios obtained from the optimizations, (16)-(17) are used to simulate gas network dynamics with the low-order solver ode15s for stiff ODE systems in MATLAB. Evaluation requires several seconds (depending on rates of change in withdrawals d) for the 24-pipe gas test network for a 24-hour period.

The results of Scenarios A, B, and C are shown in columns of Figure 2 from left to right.

Scenario A: The GFG dispatch (bottom) obtained by solving (7), the constant compression ratios (center) obtained from the static OGF, and the resulting pressure trajectories obtained from the RNF simulation (top) are given. A system pressure drop results even with the safety margin of 25%.

Scenario B: The GFG dispatch (bottom) and compression ratios (center) are the same as in Scenario #1, but tracking local pressure set-points increases the pressure constraint violation of trajectories obtained from the RNF simulation. This phenomenon can be interpreted as an amplification of cascading pressure fluctuations by a GCS that is unaware of conditions elsewhere in the GPN. When the GCS increases compression to boost downstream pressure, it aggravates upstream pressure drops.

Scenario C: The GFG dispatch solutions (bottom) and constant compressor ratios (center) differ from those for Scenarios A and B. The compression ratios are applied in the RNF simulation, and the pressure trajectories (top) are within bounds. Changes to the dispatch schedule of the electric system to maintain gas system feasibility increases the OPF cost by 5% because it changes away from the optimum.

In addition to the baseline case where constant electrical loads were scaled to 50% of nominal RTS96 model values, we also consider low and high stress cases in which this scaling is 25% and 65%, respectively. We compare the scenarios in the three stress cases by evaluating the DC OPF objective function value, the total daily gas used for generation, and the L_2 norm of pressure constraint violation of the form $v_\rho = \|V_\rho\|_2$, where

$$V_\rho = \left[\int_0^T (p(t) - p_{\max})_+^2 dt \right]^{\frac{1}{2}} + \left[\int_0^T (p_{\min} - p(t))_+^2 dt \right]^{\frac{1}{2}} \quad (28)$$

and $(x)_+ = x$ if $x \geq 0$ and $(x)_+ \equiv 0$ if $x < 0$. These

Scenario	DC OPF objective (\$ $\times 10^6$)			Pressure Violation Norm (psi-days)			GFG Gas Usage (mmBTU $\times 10^5$)		
	A	B	C	A	B	C	A	B	C
low (25%)	0.5972	0.5972	0.5971	5.5270	39.039	0.3270	2.1446	2.1446	2.1415
base (50%)	0.7316	0.7316	0.7708	104.27	137.37	0	3.0608	3.0608	3.0010
high (65%)	0.8256	0.8256	0.9961	273.01	172.55	0.0526	3.8015	3.8015	3.1697

Fig. 3. Comparison of metrics for scenarios and stress cases

metrics quantify aspects of the scenarios at various levels of system stress. Their values for the three scenarios under low, base, and high stress cases are given in the table in Figure 3. The metric v_ρ is computed using ODE solution using the RNF equations (16)-(17) embedded with the optimized compression ratios α_{ij} . The compression ratios obtained in Scenario A with the static OGF alone lead to pressure violations. Moving to Scenario C eliminates pressure constraint violations in each case, albeit at higher dispatch cost for the baseline and high cases. Using local pressure set-point tracking at compression stations (Scenario B) may worsen pressure constraint violation relative to constant ratios by amplifying spatiotemporal fluctuations that cascade through the system. Moving from Scenario A to C will improve system security but at increased generation dispatch cost, and would require substantial regulatory change.

VII. CONCLUSIONS

We have compared scenarios for separate and combined optimization for integrated electric power and natural gas infrastructures, and two gas compressor operation protocols. The performance assessment within a simulation and optimal control framework demonstrates the feasibility of computing optimal and secure solutions for these large-scale systems that interact through gas-fired generators that create large and variable gas flows. Solutions to optimization problems involving gas dynamics were investigated using physics-based continuous-time simulations to quantify the advantages of joint optimization. We also showed that when the gas system is optimized using a steady-state model, local tracking of pressure set-points by compressors increases pressure violations compared to using constant compression ratios.

ACKNOWLEDGEMENTS

We thank Russell Bent, Seth Blumsack, and Sidhant Misra for valuable discussions. Part of this work was carried out under the auspices of the NNSA of the U.S. Department of Energy at Los Alamos National Laboratory under contract #DE-AC52-06NA25396, with partial support by DTRA Basic Research Project #10027-13399, the Advanced Grid Modeling Program in the U.S. Department of Energy Office of Electricity, and project UMBRELLA under the 7th Framework Programme of the E.U., grant agreement #282775.

REFERENCES

- [1] R. Levitan et al. Pipeline to reliability: Unraveling gas and electric interdependencies across the eastern interconnection. *Power and Energy Magazine, IEEE*, 12(6):78–88, 2014.
- [2] M. Shahidepour and Z. Li. White paper: Long-term electric and natural gas infrastructure requirements. Technical report, Illinois Institute of Technology, 2014.
- [3] E. Litvinov. Design and operation of the locational marginal prices-based electricity markets. *Generation, Transmission Distribution, IET*, 4(2):315–323, February 2010.
- [4] Forward Market Operations. Energy & Ancillary Services Market Operations, M-11 Rev. 75. Technical report, PJM, 2015.
- [5] R. Rubio et al. Integrated natural gas and electricity market: A survey of the state of the art in operation planning and market issues. In *IEEE/PES Transmission and Distribution Conference and Exposition: Latin America*, pages 1–8, 2008.
- [6] MITEI. Growing concerns, possible solutions: The Interdependency of Natural Gas and Electricity Systems, 2013.
- [7] R. D. Tabors et al. Who's on first? the coordination of gas and power scheduling. *The Electricity Journal*, 25(5):8–15, 2012.
- [8] S. Thumb et al. Natural gas market regionalization and implications. Technical report, Electric Power Research Institute, 1998.
- [9] S. Misra et al. Optimal compression in natural gas networks: A geometric programming approach. *IEEE Transactions on Control of Network Systems*, 2(1):47–56, 2015.
- [10] R. Z. Ríos-Mercado and C. Borraz-Sánchez. Optimization problems in natural gas transportation systems: A state-of-the-art review. *Applied Energy*, 147:536–555, 2015.
- [11] H. Rachford and R. Carter. Optimizing pipeline control in transient gas flow. *Pipeline Simulation Interest Group*, 2000.
- [12] M. Steinbach. On PDE solution in transient optimization of gas networks. *J. of Computat. and Appl. Math.*, 203(2):345–361, 2007.
- [13] A. Zlotnik, S. Dyachenko, S. Backhaus, and M. Chertkov. Model reduction and optimization of natural gas pipeline dynamics. In *ASME Dynamic Systems and Control Conference*, page V003T39A002, Columbus, OH, 2015.
- [14] A. Zlotnik, M. Chertkov, and S. Backhaus. Optimal control of transient flow in natural gas networks. In *54th IEEE Conference on Decision and Control*, pages 4563–4570, Osaka, Japan, 2015.
- [15] S. An, Q. Li, and T. Gedra. Natural gas and electricity optimal power flow. In *IEEE PES Transmission and Distribution Conference and Exposition*, volume 1, pages 138–143. IEEE, 2003.
- [16] C. Unsihuay et al. Modeling the integrated natural gas and electricity optimal power flow. In *IEEE PES General Meeting*, pages 1–7, 2007.
- [17] C. Liu, M. Shahidepour, Y. Fu, and Z. Li. Security-constrained unit commitment with natural gas transmission constraints. *IEEE Transactions on Power Systems*, 24(3):1523–1536, 2009.
- [18] C. M. Correa-Posada and P. Sánchez. Security-constrained optimal power and natural-gas flow. *IEEE Transactions on Power Systems*, 29(4):1780–1787, 2014.
- [19] B. C. Erdener et al. An integrated simulation model for analysing electricity and gas systems. *Internat. J. of Electrical Power & Energy Systems*, 61:410–420, 2014.
- [20] M. Chaudry, N. Jenkins, and G. Strbac. Multi-time period combined gas and electricity network optimisation. *Electric Power Systems Research*, 78(7):1265–1279, 2008.
- [21] Gas-Grid Network and Case Study: <https://db.tt/yLQa2cDz>.
- [22] C. Grigg et al. The IEEE reliability test system-1996. *IEEE Transactions on Power Systems*, 14(3):1010–1020, 1999.
- [23] W. Katzenstein and J. Apt. Air emissions due to wind and solar power. *Environmental science & technology*, 43(2):253–258, 2008.
- [24] R. D. Zimmermann et al. Matpower: Steady-state operations, planning, and analysis tools for power systems research and education. *IEEE Trans. Power Systems*, 23(1):12–19, 2011.
- [25] B. Stott et al. Review of linear programming applied to power system rescheduling. In *IEEE Power Industry Computer Applications Conference*, pages 142–154, May 1979.
- [26] M. Vrakopoulou et al. Probabilistic guarantees for the N-1 security of systems with wind power generation. In *PMAPS*, Istanbul, 2012.
- [27] A. Osiadacz. Simulation of transient gas flows in networks. *International J. for Numerical Methods in Fluids*, 4:13–24, 1984.
- [28] J. Ruths, A. Zlotnik, and J.-S. Li. Convergence of a pseudospectral method for optimal control of complex dynamical systems. In *50th IEEE Conf. on Decision and Control*, pages 5553–5558. IEEE, 2011.
- [29] L. Biegler and V. Zavala. Large-scale nonlinear programming using IPOPT: An integrating framework for enterprise-wide dynamic optimization. *Computers & Chem. Eng.*, 33(3):575–582, 2009.